

## Effective properties of amorphous metamaterials

C. Helgert,<sup>1</sup> C. Rockstuhl,<sup>2</sup> C. Etrich,<sup>1</sup> C. Menzel,<sup>2</sup> E.-B. Kley,<sup>1</sup> A. Tünnermann,<sup>1</sup> F. Lederer,<sup>2</sup> and T. Pertsch<sup>1</sup>

<sup>1</sup>*Institute of Applied Physics, Friedrich-Schiller-Universität Jena, Max-Wien-Platz 1, D-07743 Jena, Germany*

<sup>2</sup>*Institute of Condensed Matter Theory and Solid State Optics, Friedrich-Schiller-Universität Jena,*

*Max-Wien-Platz 1, D-07743 Jena, Germany*

(Received 8 April 2009; revised manuscript received 20 May 2009; published 26 June 2009)

We experimentally and numerically study the propagation of light through amorphous metamaterials. For this purpose we introduce a precisely controllable degree of positional disorder into a perfectly periodic system, transforming it to a partially disordered and ultimately an amorphous metamaterial. The observable spectral features occurring upon this transition and the impact of coherent interactions among neighboring unit cells are revealed. Backed by numerical simulations, the effective properties of the metamaterials are retrieved, most notably for the amorphous one. The most important finding with respect to negative index materials is that their magnetic properties are not affected by an arbitrarily high degree of disorder. This work enables the quantitative evaluation of effective properties of amorphous metamaterials fabricated by bottom-up approaches.

DOI: [10.1103/PhysRevB.79.233107](https://doi.org/10.1103/PhysRevB.79.233107)

PACS number(s): 78.20.Ci, 73.20.Mf, 75.30.Kz, 78.20.Ek

Photonic metamaterials (MMs) attract an ever growing interest from both theoretical and experimental sides. They derive their fascination from the promise to observe unprecedented electromagnetic material properties such as optical magnetism or negative refraction. MMs with such properties will fundamentally alter our perception of light propagation and permit for groundbreaking applications such as sub-wavelength imaging<sup>1</sup> or cloaking devices.<sup>2</sup> The proof-of-principle experiments for optical MMs were performed using thin films of laterally patterned nanostructures.<sup>3,4</sup> For the sake of technological and numerical feasibilities the vast majority of these subwavelength structures were only investigated in periodic arrangements. The spectroscopic properties of such crystalline MMs were then compared to numerical simulations of periodically repeated single unit cells. From the measured and/or simulated complex reflected and transmitted amplitudes at such slabs the effective properties, such as the effective permittivity and the effective permeability, can be retrieved at normal<sup>5</sup> or oblique incidence including the influence of the substrate.<sup>6</sup> The physical origin of the observed dispersion in either effective property is usually explained by the peculiar scattering properties of the meta-atom that constitutes the unit cell, where the periodic arrangement is disregarded and merely understood as a parameter that dictates the filling fraction and hence the strength of the induced dispersion of the effective properties. Nonetheless, to fully support such an understanding of MMs one has to probe for their properties if the meta-atoms are not arranged along a lattice. Such investigations in terms of effective properties of truly amorphous MMs have not been reported to date mainly due to the limitations imposed by computational facilities to treat them rigorously.

The quantitative investigation of amorphous MMs is urgently in need for two practical reasons. At first, the vast majority of current MMs is fabricated by costly and time-consuming serial writing processes such as laser or electron-beam lithography. It hinders the transfer of fundamental MM concepts from an academic toward an industrial environment where true applications shall be implemented. Quick and reliable fabrication schemes based on self-assembling or

chemically randomized processes will ease the applicability of large-scale MMs.<sup>7</sup> At second, in order to incorporate a potentially negative-index MM into an imaging application, it ought to show a weak spatial dispersion.<sup>8</sup> However, the mesoscopic arrangement of meta-atoms in most of the present MMs causes inevitably a high degree of anisotropy and strong spatial dispersion.<sup>9</sup> These constraints can be lifted by employing amorphous MMs. The study of disordered photonic systems such as metallic nanoapertures,<sup>10</sup> metallic gratings,<sup>11</sup> and photonic crystals<sup>12</sup> has gained a growing interest recently. As for MMs, both dimensional<sup>13</sup> and positional disorders<sup>14</sup> have been addressed. However, no effective properties have been assigned to disordered MMs yet. Accordingly the question arises whether a magnetic resonance will be retained if lithographically fabricated MMs are substituted by bottom-up approaches.

In this contribution we retrieve the effective properties for a prototypical near-infrared MM upon its transition from a crystalline to an amorphous structure. The considered meta-atom consists of a cut-wire pair.<sup>3,4</sup> Since each cut-wire supports a localized plasmon polariton, their strong coupling causes a splitting of the resonance into a symmetric and an antisymmetric mode. Since for the high-frequency symmetric mode the current densities in both arms are in phase, it effectively acts as an electric dipole, hence inducing a Lorentzian dispersion in the effective permittivity. By contrast, the current densities in both arms oscillate  $\pi$  out of phase for the low-frequency antisymmetric mode evoking an electric quadrupole and a magnetic dipole moment and cause a Lorentzian dispersion in the effective permeability.<sup>15</sup> The latter is crucial to obtain a negative index material. The transition from a crystalline to an amorphous MM is implemented by introducing an increasing amount of positional disorder. In the amorphous system short-range as well as long-range correlations in the spatial positions of the meta-atoms will vanish. A predominant nearest-neighbor interaction is suppressed by introducing a required minimal distance among adjacent unit cells.<sup>10</sup> We demonstrate that the two spectral resonances show a dramatically different characteristic when the system modified by disorder. We provide

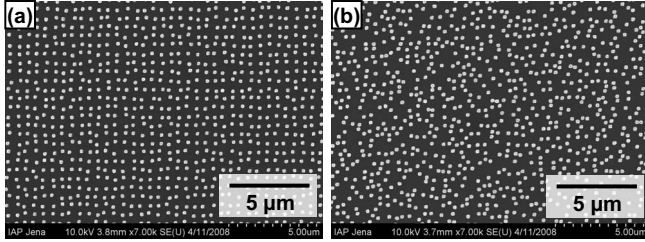


FIG. 1. Normal view SEM micrographs of the fabricated MMs with disorder parameter (a)  $D_5=0.4$  and (b)  $D_7=1.6$ .

a comprehensive physical explanation in terms of the single-element scattering response for this observation, retrieve the effective properties of the MM along its transition from a crystalline to an amorphous medium and discuss implications for potential applications.

Following the common approach,<sup>14</sup> we introduce uncorrelated positional disorder into the system by displacing each cut-wire pair from its original position on a perfect quadratic grid by adding a uniformly distributed spatial disorder. It is randomly chosen from the interval  $\Delta x \in [-\frac{Dp}{2}, +\frac{Dp}{2}]$  and  $\Delta y \in [-\frac{Dp}{2}, +\frac{Dp}{2}]$ , where  $D$  is a dimensionless disorder parameter and  $p$  is the lattice constant of the periodic system. The cut-wire pair samples were fabricated on top of a fused silica substrate covered by 10 nm of indium-tin oxide. The width of the cut-wire pairs in both lateral directions is 180 nm. Vertically, they consist of two 30 nm gold layers separated by a 45 nm magnesia spacer. In the referential periodic sample, the lattice constant is 512 nm for both lateral dimensions. Using electron-beam lithography, we were able to precisely control the nanostructure positions. Eleven samples with increasing disorder parameters ( $D_1=0$ ,  $D_2=0.02$ ,  $D_3=0.08$ ,  $D_4=0.2$ ,  $D_5=0.4$ ,  $D_6=0.8$ ,  $D_7=1.6$ ,  $D_8=7.8$ ,  $D_9=15.6$ ,  $D_{10}=78$ , and  $D_{11}=1000$ ) were fabricated. Each sample extended over an area of 9 mm<sup>2</sup>. The overall number of cut-wire pairs in the system was kept constant. To avoid strong near-field coupling of neighboring meta-atoms and a resulting inhomogeneous spectral-line broadening, a minimum separation of 66 nm was enforced. Otherwise, the resonance properties of the individual meta-atoms would have been predominantly affected causing an inhomogeneous line broadening. Moreover, this minimal separation shall fairly reflect standard routines to fabricate self-organized MMs using, e.g., charged colloidal beads. Accordingly, we are able to evaluate experimentally the gradual transition from a crystalline (corresponding to  $D_1$ ) to an amorphous MM (corresponding to  $D_{11}$ ). Two representative electron microscope pictures of the samples with  $D_5=0.4$  and  $D_7=1.6$  are shown in Fig. 1.

The optical properties of all samples were characterized by transmission and reflection spectroscopy with a Perkin-Elmer Lambda950. At normal incidence identical results have been obtained for both linear polarization states parallel to either lattice vector. The investigated spectral domain ranged from 500 to 1200 nm, comprising all relevant resonances of the system. The spectral results are shown in Fig. 2. For the periodic arrangement ( $D=0$ ) two dips appear in the transmission spectrum situated at 800 and 1050 nm which are related to the symmetric and antisymmetric plas-

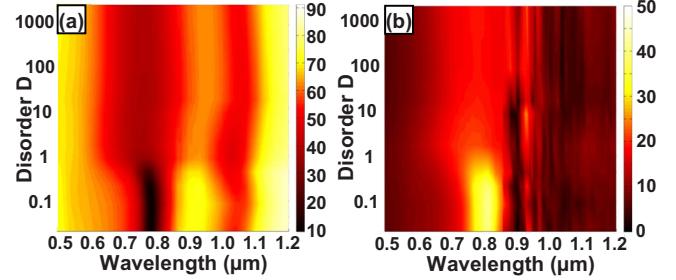


FIG. 2. (Color online) (a) Measured transmission (b) and reflection as a function of the wavelength and the disorder parameter  $D$  (logarithmic scale). Both spectra are recorded for discrete values of  $D$  and interpolated for convenience.

mon polariton eigenmodes of the cut-wire pair. The former is confirmed by a noticeable peak in reflection at 800 nm. A considerably different behavior may be observed for an increasing degree of disorder. While the antisymmetric resonance at 1050 nm almost perfectly sustains in width and magnitude even for  $D=1000$ , the symmetric resonance blue-shifts by about 30 nm, broadens and its magnitude decays already at a moderate level of disorder ( $D=1$ ). The low signal-to-noise ratio in the range from 900 to 1000 nm in the reflection spectra is due to low sensitivity of the detector and does not bear any physical meaning.

To compare these spectra with theoretical predictions, we performed finite-difference time-domain simulations<sup>16</sup> of the system for no ( $D=0$ ), moderate ( $D=0.3$ ), and high ( $D=3$ ) positional disorders. We have restricted our simulations to a sufficiently large supercell containing 196 cut-wire pairs with a size of  $7 \times 7 \mu\text{m}^2$ . All parameters for the simulations were taken from the measured nanostructure topography and a linearly polarized plane wave at normal incidence was assumed. Simulations for a set of discrete wavelengths were performed taking into account the dispersion of gold according to Ref. 17. The refractive indices of the substrate and of MgO were assumed to be 1.5 and 1.72, respectively. The

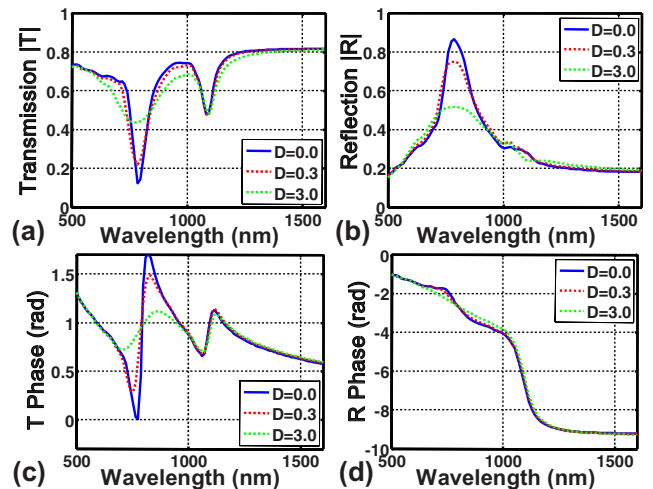


FIG. 3. (Color online) Simulated (a) modulus of transmission, (b) modulus of reflection, (c) transmission phase delay, and (d) reflection phase delay of the cut-wire pair MM as a function of the wavelength.

supercell was truncated by periodic boundaries in the lateral dimensions whereas perfectly matched layers were used along the propagation direction. To obtain the spectral response, the transmitted and reflected components of the illuminating wave were extracted and Fourier transformed. We only took the zeroth diffraction order into account. Figure 3 shows the simulated spectra for the three scenarios. The magnitude and the phase are shown for transmission and reflection. The two aforementioned plasmonic resonances appearing at 800 and 1050 nm for  $D=0$  are confirmed. Their identification as the symmetric and antisymmetric eigenmodes of the cut-wire pair structure is supported by supplementary investigation of the near-field at the resonant wavelengths (not shown for brevity). Moreover, all experimental observations in transmission and reflection that occur for an increasing degree of disorder are fully reproduced. With  $D$  increasing, the symmetric resonance at 800 nm broadens, blueshifts, decays, and nearly vanishes already for  $D=3$ . This evolution does not apply for the antisymmetric eigenmode at 1050 nm. While  $D$  increases, the dip in the transmitted amplitude and its corresponding phase evolution retain their strength and width almost perfectly. Hence, the antisymmetric eigenmode is nearly invulnerable to positional disorder.

These different characteristics can be explained considering the peculiarities of the two eigenmodes. For the high-frequency symmetric eigenmode the two cut-wires act as an electric dipole. In the lateral plane of the MM the scattered field of both dipoles always interferes constructively. Most notably, it causes a strong field that is polarized along the incidence polarization. Therefore, the local electric field driving each meta-atom consists of the illuminating external field superimposed by the field scattered from all meta-atoms. In the periodical arrangement this is not detrimental since the illumination conditions are identical for all meta-atoms in the lattice. However, upon the transition to the amorphous state, the scattered fields from all meta-atoms lose their fixed phase relation and their individual driving forces are modified. The results are a strong homogeneous line broadening and a resonance damping.<sup>18</sup> By contrast, applying these arguments to the antisymmetric low-frequency mode provides complementary results. As already discussed out of phase dipole oscillations generate a scattered field which is dominated by an electric quadrupole and a magnetic dipole contribution.<sup>19</sup> However, in the lateral plane of the MM both multipoles lack an in-plane polarized field component due to destructive interference of the scattered field from the upper and the lower cut wires. The only nonzero field component in the lateral plane is that normal to the substrate. Since the cut-wire pair sustains only a resonant response for in-plane field components, this scattered field has no influence. Therefore, the driving force of each meta-atom is solely the external illumination and the spectral response is independent of the arrangement.

Based on the remarkable agreement between measured and simulated spectra, we retrieve effective properties for the periodic, the weakly disordered, and the amorphous MM. Relying on the computed complex reflection and transmission spectra at normal incidence we apply a retrieval algorithm.<sup>6</sup> In Fig. 4, the real and imaginary parts of the

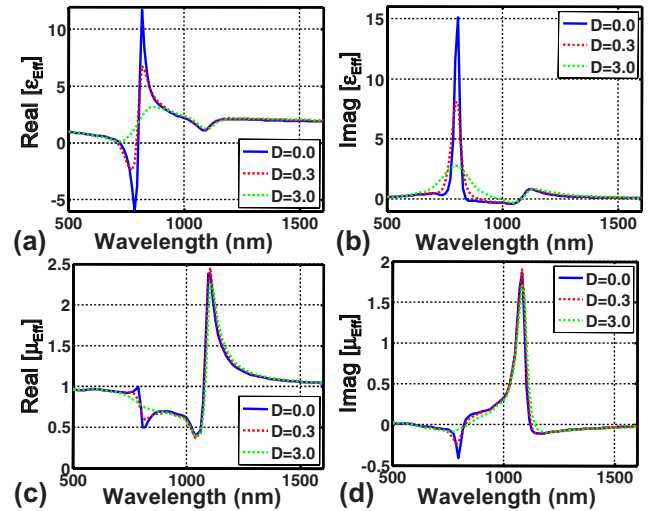


FIG. 4. (Color online) Wavelength-dependent effective properties of the cut-wire pair MM. (a) Real and (b) imaginary parts of the effective permittivity and (c) real and (d) imaginary parts of the effective permeability.

effective permittivity and permeability are plotted versus the wavelength for the three disorder parameters  $D=0$ ,  $D=0.3$ , and  $D=3$ . For the periodic case ( $D=0$ ), we identify the two relevant resonances causing a Lorentzian dispersion in the effective permittivity (permeability) for the high-(low-) frequency (anti)symmetric eigenmode. The high-frequency resonance that induces a Lorentzian dispersion of the effective permittivity strongly degrades with increasing disorder. Since the electric dipoles excited in the meta-atoms cease to oscillate in phase the resonance is homogeneously broadened, causing a degradation of the induced dispersion. For the amorphous MM the real part of the effective permittivity becomes positive. Another important finding concerns the antiresonance in the effective permeability that comes along with the resonance in the effective permittivity. It is usually regarded as an artifact of the periodical arrangement of the unit cells. Here it is clearly shown that it indeed degrades strongly and is hardly discernible for the amorphous MM. In contrast to the permittivity, the effective permeability related to the antisymmetric eigenmode does not experience appreciable changes. Independent of the degree of disorder the line shape, the strength, and the width of this resonance remain preserved. Thus the magnetic response of the MM is solely determined by the response of the individual meta-atoms regardless of their arrangement. This is an amazingly encouraging result because optical negative index MMs require only a strong resonant magnetic response, provided, e.g., by an electric quadrupole contribution, whereas the negative permittivity may be provided by a nonresonant metallic background. From these findings we may conclude that the effective optical properties of most of current negative-index MM are only marginally affected by the arrangement of the meta-atoms. This is of primary importance for MMs fabricated by self-organized bottom-up approaches. We emphasize that already for  $D=3$  all effects inherent to the periodic MM are nullified and the MM exhibits all features of a truly amorphous MM.

In conclusion, we have investigated the propagation of light through amorphous cut-wire pair MMs at near-infrared frequencies. Departing from a perfectly periodic system, we experimentally demonstrated that the spectral location, the strength, and the width of the antisymmetric eigenmode are not affected by an arbitrary degree of positional disorder. On the contrary, the symmetric eigenmode of the same nanostructure suffers strongly from disorder and decays rapidly when the periodic arrangement of the meta-atoms degrades. A comprehensive explanation of these phenomena was given on the basis of the cut-wire pair eigenmodes and their resulting in-plane interactions. We retrieved and compared the effective properties of periodic, partially disordered, and amorphous MMs. To the best of our knowledge, this approach has not been reported so far. One key finding is the insensitivity of the magnetic resonance against positional disorder. Thus

such disorder does not affect the principal optical functionality of optical negative-index MMs. The second key finding is the degradation of all features that are counterintuitive to our physical picture such as an antiresonance in any of the effective properties. Our findings have important implications for the integration of optical negative-index MMs in subwavelength imaging applications and relax the strong limitation of the necessity of periodicity in modern MM design concepts.

We thank K. Fuechsel (IOF Jena) and B. Steinbach (IPHT Jena) for providing us with thin films. Financial support by the Federal Ministry of Education and Research (Unternehmen Region, ZIK ultraoptics, Grant No. 13N9155 and Metamat) and the Thuringian State Government (MeMa) is acknowledged.

- 
- <sup>1</sup>J. B. Pendry, *Phys. Rev. Lett.* **85**, 3966 (2000).  
<sup>2</sup>D. Schurig, J. Mock, B. Justice, S. Cummer, J. Pendry, A. Starr, and D. Smith, *Science* **314**, 977 (2006).  
<sup>3</sup>V. Shalaev, W. Cai, U. Chettiar, H. Yuan, A. Sarychev, V. Drachev, and A. Kildishev, *Opt. Lett.* **30**, 3356 (2005).  
<sup>4</sup>G. Dolling, C. Enkrich, M. Wegener, J. F. Zhou, C. M. Soukoulis, and S. Linden, *Opt. Lett.* **30**, 3198 (2005).  
<sup>5</sup>D. R. Smith, S. Schultz, P. Markos, and C. M. Soukoulis, *Phys. Rev. B* **65**, 195104 (2002).  
<sup>6</sup>C. Menzel, C. Rockstuhl, T. Paul, F. Lederer, and T. Pertsch, *Phys. Rev. B* **77**, 195328 (2008).  
<sup>7</sup>T. Pakizeh, A. Dmitriev, M. S. Abrishamian, N. Granpayeh, and M. Käll, *J. Opt. Soc. Am. B* **25**, 659 (2008).  
<sup>8</sup>T. Paul, C. Rockstuhl, C. Menzel, and F. Lederer, *Phys. Rev. B* **79**, 115430 (2009).  
<sup>9</sup>C. R. Simovski, *Metamaterials* **2**, 169 (2008).  
<sup>10</sup>C. Rockstuhl, F. Lederer, T. Zentgraf, and H. Giessen, *Appl. Phys. Lett.* **91**, 151109 (2007).  
<sup>11</sup>B. Auguié and W. L. Barnes, *Opt. Lett.* **34**, 401 (2009).  
<sup>12</sup>R. Rengarajan, D. Mittleman, C. Rich, and V. Colvin, *Phys. Rev. E* **71**, 016615 (2005).  
<sup>13</sup>M. Gorkunov, S. A. Gredeskul, I. V. Shadrivov, and Y. S. Kivshar, *Phys. Rev. E* **73**, 056605 (2006).  
<sup>14</sup>N. Papasimakis, V. Fedotov, Y. Fu, D. Tsai, and N. Zheludev, arXiv:0809.2361 (unpublished).  
<sup>15</sup>J. Petschulat, C. Menzel, A. Chipouline, C. Rockstuhl, A. Tünnermann, F. Lederer, and T. Pertsch, *Phys. Rev. A* **78**, 043811 (2008).  
<sup>16</sup>A. Taflove and S. Hagness, *Computational Electrodynamics: The Finite-Difference Time-Domain Method*, 3rd ed. (Artech House, Boston, 2005).  
<sup>17</sup>P. Johnson and R. Christy, *Phys. Rev. B* **6**, 4370 (1972).  
<sup>18</sup>S. Zou and G. Schatz, *J. Chem. Phys.* **121**, 12606 (2004).  
<sup>19</sup>D. J. Cho, F. Wang, X. Zhang, and Y. R. Shen, *Phys. Rev. B* **78**, 121101(R) (2008).